NJC

ROYAL SOCIETY OF CHEMISTRY

PAPER

View Article Online
View Journal | View Issue

Cite this: *New J. Chem.*, 2023, **47**, 11919

Oxytetracycline-derived carbon dots as a fluorescent switch in trace ferric ion sensing†

Tao Chen,‡[abcd] Yan-Tong Xu,‡[bcd] Qing Guo,[abcd] Xiaoli Chen,[bcd] Qiucheng Su[bcd] and Yan Cao*[abcd]

Received 26th April 2023,
Accepted 31st May 2023

DOI: 10.1039/d3nj01930f

rsc.li/njc

The analysis of trace Fe(III) ions in water is of vital importance in the fields of biology, environment and health. The fluorescent switch technique based on photoluminescent carbon dots (CDs) is highly favorable due to their bio-adaptability, safety and economy, but it is hindered in the highly specific recognition at the trace level. In this work, oxytetracycline-derived CDs (denoted as OCDs) with a uniform size (*ca.* 2.04 nm), nitrogen dopant, and rich hydroxyl-/carboxyl- groups have been successfully fabricated *via* a bottom-up hydrothermal carbonization approach. The as-prepared OCDs have displayed excellent photoluminescence characteristics and fluorescence switch performance for the rapid detection of Fe(III) within 2 min with the limit of detection (LOD) as low as 0.440 μM (24.6 ppb) and the second highest sensitivity of 3.52×10^{-2} μM^{-1} among reported CDs-based Fe(III) fluorescent switch materials. This detection system is stable in the analysis matrix with many interfering metal ions, at least with the help of the masking agent cysteine, realizing the specific detection of Fe(III) in real water environments. The contributions from the fluorophore concentration and the affinity between fluorophore and quencher have been revealed by the numerical model, providing a roadmap for the design of metal ion fluorescence switch materials based on a complex formation quenching mechanism. Fluorescence cell imaging in plant cells has also been performed successfully with the as-synthesized OCDs. This work presents a high-performing CDs-based Fe(III) fluorescence switch derived from the environmentally-risky oxytetracycline, as well as a feasible strategy for recycling waste antibiotics.

Introduction

The explosive growth of trace analysis in various fields (electronics, biology, medical diagnostics, environments and so on) demands more selective, sensitive, rapid, convenient, safe, adaptable and economical detection methods. For example, it is now highly demanding to develop ferric ion (Fe(III)) detection methods because of the important role of Fe(III) in biochemical and environmental processes (such as cellular metabolism, enzyme catalysis, electron transfer, oxidation reactions and oxygen transport[1–4]). The concentration of Fe(III) in water has become an important indicator in the quality assessment of the water environment and ecology. The sources of Fe(III) pollution are mainly the water corrosion of steel and discharged industrial wastewater,[5,6] potentially threatening domestic water systems and human health. The U.S. Environmental Protection Agency (EPA) has regulated the maximum allowable level of Fe(III) in drinking water to be 0.3 mg L^{-1} (equivalent to 5.4 μM).[7,8]

Among the available trace analysis methods for Fe(III), fluorescence technology exhibits greater advantages in terms of rapidness, convenience and economics, but not always in sensitivity ($dQE/dc_{Fe(III)}$, QE = quenching efficiency), selectivity, safety and adaptability, when compared to mass spectrometry (MS),[9] voltammetry,[10] liquid chromatography (LC),[11] and atomic absorption spectroscopy (AAS).[12] Carbon dots (CDs) are next-generation photoluminescent nanomaterials that provide remarkable fluorescence properties,[13] with less toxicity,[14,15] better biocompatibility[16,17] and lower cost.[18,19] Currently, CDs are widely used as fluorescent probes for the detection of various molecules or ions, such as metal ions, nucleic acids, enzymes, proteins, explosives and so on.[20–23] For the specific detection of Fe(III), Lee *et al.* prepared *Magnolia liliiflora*-derived nitrogen-doped CDs (N-CDs); their fluorescence can be switched off by Fe(III), exhibiting a good linear response to the concentration of

[a] *College of Chemistry and Chemical Engineering, Anhui University, Hefei 230601, China. E-mail: caoyan@ms.giec.ac.cn*
[b] *Guangzhou Institute of Energy Conversion, Chinese Academy of Sciences, Guangzhou 510640, China*
[c] *Guangdong Provincial Key Laboratory of New and Renewable Energy Research and Development, Guangzhou 510640, China*
[d] *CAS Key Laboratory of Renewable Energy, Guangzhou 510640, China*

† Electronic supplementary information (ESI) available. See DOI: https://doi.org/10.1039/d3nj01930f

‡ These authors contributed equally to this work.

Fe(III) but less sensitive (about 50% of fluorescence quenching in 250 μM Fe(III)).[3] This sensitivity is too low to satisfy the demand for trace and precise detection. Therefore, the development of more high-performing CDs is a high priority, especially in the pursuit of advanced fluorescent switch materials for selective and sensitive Fe(III) detection.

The functionality of high-performing CDs is determined by their precursors and preparation methods. Some macromolecules such as biomass precursors, typically laboratory waste paper *via* the hydrothermal carbonization (HTC) route, exhibited an Fe(III) luminescence sensing range of 5–250 mM,[18] which was further improved to 1–50 μM using food waste.[24] However, their unfavorable sensitivities do not meet the requirements for trace analysis. To further improve the performance and designability of CDs, small molecule-based bottom-up carbonization has been developed, which can partially reserve heteroatoms and functional groups on precursor molecules and is more attractive for controllably fabricating functionalized CDs as compared to the macromolecule precursor-based top-down approach.[25–27] For example, using citric acid, 1-aminopropyl-3-methylimidazolium-functionalized CDs were achieved *via* microwave-assisted HTC, which exhibited a sensitivity of 1.27×10^{-3} μM^{-1} for Fe(III).[28] As is well known, the phosphorus and chlorine co-doped CDs (P, Cl-CDs) prepared from the hydroxyl-rich maltose displayed the highest quenching sensitivity of 0.0566 μM^{-1} in the Fe(III) range of 0.1–8 μM; however, it became less sensitive above 8 μM, and the quenching efficiency (QE) was less than 70% even above 100 μM of Fe(III).[29] This indicates that the bottom-up carbonization using small molecule precursors, especially introducing heteroatom dopants and coordinating groups (such as –COOH), may be the means for the rational design and preparation of advanced CD materials.

Considering the specific coordination between Fe(III) and the phenolic hydroxyl group, the increase in the hydroxyl content on the CD surface is supposed to be helpful in the significant improvement of the sensitivity of fluorescent CDs in Fe(III) sensing. Oxytetracycline, a small-molecule antibiotic that is a potential environmental waste and hazard, contains abundant hydroxyl groups and nitrogen atoms suitable for CD preparation.[30] We have successfully used oxytetracycline to achieve the fabrication of CDs (denoted as OCDs) with a controllable and uniform size (*ca.* 2.04 nm), nitrogen dopant, and rich hydroxyl-/carboxyl- groups *via* a quick and convenient bottom-up HTC approach, displaying superior stability, water solubility and bright photoluminescence (Fig. 1). Compared with the reaction conditions of other bottom-up methods (Table S1, ESI†), this method is the most rapid and convenient method for preparing CDs. Simultaneously, the as-synthesized OCDs can be used as fluorescence switches for the detection of Fe(III), not only selectively distinguishing out (III) from Fe(II), but also sensitively achieving a LOD as low as 0.440 μM (24.6 ppb). More importantly, its sensitivity reached 3.52×10^{-2} μM^{-1}, which is the second highest among CDs. With a technique using the masking agent cysteine, the as-prepared OCDs can further expand their usefulness and feasibility in the specific detection of Fe(III) in real water environments such as lake water, where there are many interfering metal ions. The complexing mechanism has been proved by the proposed numerical model, providing a design roadmap for metal ion fluorescence switch materials based on a complex formation quenching mechanism. Fluorescence cell imaging in plant cells has also been achieved with the as-synthesized OCDs. This work addresses a high-performing CDs-based Fe(III) fluorescence switch derived from the environmentally-risky oxytetracycline, as well as a feasible strategy for recycling waste antibiotics.

Experimental section

Chemicals and materials

All chemical reagents were purchased from Aladdin Industries Co. and directly used without further purification. Solutions were prepared using deionized water unless otherwise noted.

Preparation of oxytetracycline-derived carbon dots (OCDs)

Here, 50 mg of oxytetracycline was dissolved in 100 mL of deionized water and ultrasonicated for 2 h. The well-dispersed homogeneous solution was transferred to a Teflon-lined autoclave and heated at 180 °C for 1 h. The crude product was filtered through a 0.22 μm membrane to remove large particles. Subsequently, dialysis was conducted on the filtrate solution using a 1000 Da dialysis bag for three days. After purification, the filtrate was concentrated by rotary evaporation and then freeze-dried to obtain solid products of carbon dots.

The fluorescence detection of metal ions

Taking Fe(III) as an example, 5 mg of OCDs were dissolved in 100 mL of deionized water to form a homogeneous dispersion. Then, 10 μL of Fe(III)-containing aqueous solution at a

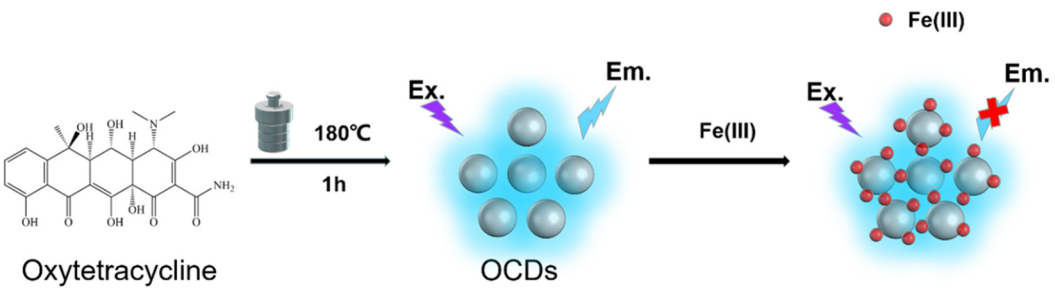

Fig. 1 Scheme showing the preparation of OCDs as the fluorescent switch for Fe(III).

concentration of 0.02 M was mixed with 2 mL of as-prepared OCDs dispersion in a quartz cuvette, and after 2 min, excited by 320 nm light for fluorescence detection. The same procedure and fluorescence conditions were also carried out for other metal ions including Al(III), Ba(II), Ca(II), Cd(II), Co(II), Fe(II), Fe(III), Hg(II), K(I), Mg(II), Mn(II), Na(I), Ni(II), Pb(II) and Zn(II).

The quenching efficiency (QE) was calculated according to eqn (1):

$$QE = (I_0 - I)/I_0 \times 100\% \quad (1)$$

where I_0 and I represent the fluorescence intensity of OCD samples without and with Fe(III) ions, respectively.

The sensitivity of OCDs for Fe(III) detection was calculated according to eqn (2):

$$\text{Sensitivity} = dQE/dc_{Fe(III)} \quad (2)$$

where $c_{Fe(III)}$ is the concentration of Fe(III) ions.

The detection limit of OCDs with Fe(III) was calculated using eqn (3),

$$LOD = 3\sigma/S \quad (3)$$

where σ is the standard deviation ($N = 11$, Fig. S1, ESI†), and S is the slope of the linear calibration plot.

Selective detection of Fe(III) using cysteine as the masking agent

Taking Hg(II) as an example, 5 mg of OCDs were dissolved in 100 mL of deionized water to form a homogeneous dispersion. Then, 10 μL Hg(II)-containing aqueous solution at a concentration of 0.02 M was mixed with 2 mL as-prepared OCD dispersion in a quartz cuvette, followed by the addition of 10 μL of cysteine solution at a concentration of 0.06 M. After 2 min, the fluorescence detection was performed with excitation at 320 nm. The same procedure and fluorescence conditions were also carried out for other metal ions, including Al(III), Ba(II), Ca(II), Cd(II), Co(II), Fe(II), Fe(III), Hg(II), K(I), Mg(II), Mn(II), Na(I), Ni(II), Pb(II) and Zn(II).

Anti-interfering performance evaluation

Taking Hg(II) as an example, 5 mg of OCDs was dissolved in 100 mL of deionized water to form a homogeneous dispersion. Then, 10 μL of Fe(III)-containing aqueous solution at a concentration of 0.02 M and 10 μL of cysteine solution at a concentration of 0.06 M were mixed with 2 mL as-mentioned OCDs solution in a quartz cuvette, followed by the addition of 10 μL Hg(II)-containing aqueous solution at a concentration of 0.02 M. After 2 min, the fluorescence detection was performed with excitation at 320 nm. The same procedure and fluorescence conditions were also conducted for other metal ions, including Al(III), Ba(II), Ca(II), Cd(II), Co(II), Fe(II), Hg(II), K(I), Mg(II), Mn(II), Na(I), Ni(II), Pb(II) and Zn(II).

Detection of Fe(III) in real lake water

The real lake water was sampled from Emerald Lake in Hefei, China. The solid impurities in the as-collected lake water were removed by centrifugation and filtration prior to use. A solution of Fe(III) with a concentration of 2.5–60 μM was prepared using lake water as the solvent. Next, 5 mg of OCDs were dissolved in 100 mL of deionized water to form a homogeneous dispersion. Then 10 μL of the lake water solution containing Fe(III) was mixed with 2 mL of the above OCDs solution in a quartz cuvette for 2 min and then excited at 320 nm for fluorescence detection.

Fluorescence imaging in plant cells

Potatoes, bean sprouts and winter squash were sliced, 100 μL of OCDs solution was added dropwise to the slices and allowed to soak for 5 min, and then the soaked slices were rinsed five times with deionized water, followed by the dropwise addition of 100 μL of Fe(III) ion solution with a concentration of 0.02 mol·L^{-1}. The resolution of the electron eyepiece of the fluorescence microscope was set to 2592 × 1944 with a magnification of about 60 times and the magnification of the fluorescence eyepiece was 60 times.

Results and discussion

Structural characterization of OCDs

For the bottom-up fabrication of carbon dots, oxytetracycline was used as the carbon source through a one-step hydrothermal carbonization route to produce blue-emitting oxytetracycline-derived carbon dots (OCDs, Fig. 2a). The quantum yield (QY) of OCDs was calculated as 1.67% using quinine sulfate in 0.1 M H_2SO_4 as a standard reference (eqn (S1), ESI†). The product yield (PY) of OCDs was calculated (eqn (S2), ESI†) as 48%. Its transmission electron microscopy (TEM, Fig. 2b) image displayed its spherical morphology and uniform size distribution (Fig. 2c) with an average diameter of 2.04 nm. The lattice spacing of the as-prepared OCDs was measured to be 0.21 nm based on its high-resolution transmission electron microscopy (HRTEM, Fig. S2, ESI†) image, which is featured as the lattice spacing of the (100) plane of the graphitic carbon.

The graphitization/crystallinity of OCDs was studied by X-ray diffraction (XRD) and Raman spectroscopy. The XRD pattern (Fig. S3, ESI†) of the OCDs showed that the diffraction peaks were located at $2\theta = 25.3^\circ$ and 42.5°, which correspond to the graphite[002] plane and the graphite[100] plane,[31–33] consistent with the high-resolution TEM analysis. The Raman spectrum of OCDs indicated a comparatively appropriate graphitization degree (I_D/I_G) of 0.92, which was calculated from the intensities of the disorder band (D band, vibrations of disordered amorphous carbon) at 1366 cm^{-1} and the crystalline graphitic band (G band, vibrations of crystalline graphite) at 1585 cm^{-1} (Fig. 2d).[34,35] The characteristic functional groups on the OCDs were identified by Fourier transform infrared (FT-IR) spectroscopy (Fig. 2e and Fig. S4, ESI†). The peaks of $\nu_{C=O}$ (1632 cm^{-1}), ν_{O-H} (about 3400 cm^{-1}), δ_{O-H} (1350 cm^{-1}), and δ_{C-O-H} (765 cm^{-1}) helped to confirm the presence of carboxyl (–COOH) and phenolic hydroxyl (–OH) groups,[24,35] Since the process of carbon dot formation includes oxidation and carbonation,[36] it is possible for carboxyl groups to appear in OCDs. The vibration peaks of N–H (3200–3400 cm^{-1}) and C–N (1383 cm^{-1}) indicate the presence of the amino group (–NH_2).[37,38] X-ray photoelectron spectroscopy (XPS, Fig. S5, ESI†) further confirmed the presence of –COOH, –OH and –NH_2 groups on the OCDs. In the high-resolution C1s

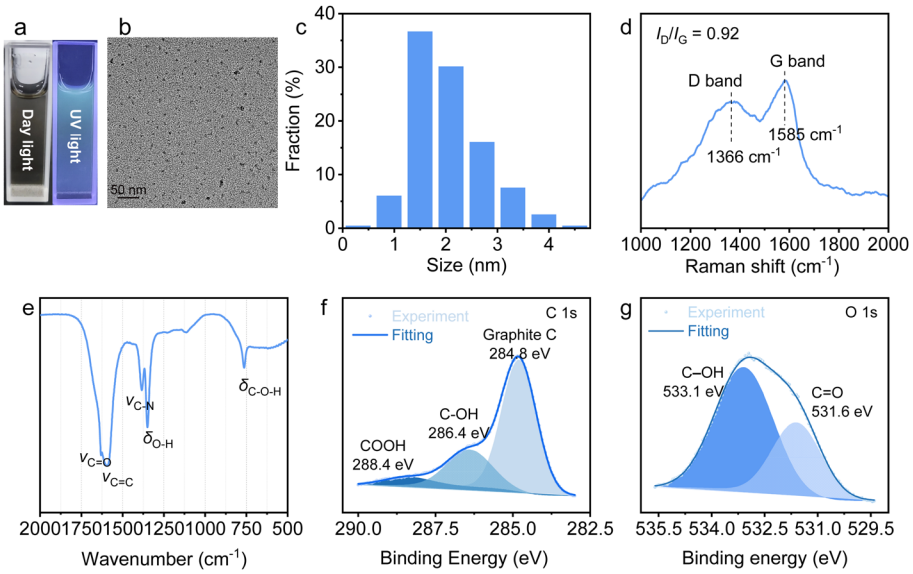

Fig. 2 Characterizations of OCDs. (a) Optical photographs under daylight and UV light; (b) TEM image and (c) the corresponding size distribution; (d) Raman spectrum; (e) FT-IR spectra; high-resolution (f) C1s and (g) O1s XPS profiles.

spectrum (Fig. 2f), three peaks at 284.8, 286.4, and 288.4 eV are attributed to three types of carbon atoms, namely, graphite C, C–OH, and COOH, respectively.[39,40] The O1s signals at 533.08 (C–O) and 531.6 eV (C═O) consist of phenolic hydroxyl and carboxyl groups (Fig. 2g).[41,42] The high-resolution N1s XPS profile is shown in Fig. S6 (ESI†). The material characterizations demonstrated that the as-synthesized OCDs contain abundant carboxyl/hydroxyl groups on their surface, which likely facilitate its coordination with the targeted Fe(III) ions, and are also likely beneficial for satisfactory hydrophilicity for its good dispersion in water for a long period.

Fluorescence properties of the OCDs

The fluorescence properties of the as-prepared OCDs were investigated using fluorescence spectroscopy. The fluorescence spectrum at 400 nm is shown in Fig. 3a, which was obtained according to the emission spectra under excitation wavelengths from 270 to 360 nm (Fig. S7, ESI†). It was found that the optimal excitation wavelength for OCDs was 320 nm to achieve the maximal fluorescence intensity. That shift in the maximal emission wavelengths at around 400 nm was negligible with varied excitation wavelengths, implying the independent emission wavelength of OCDs on excitation. This was notably different from most reported CDs.[43] Such emission behavior with unchanged wavelength under different excitation wavelengths provides reliable stability when applied as a fluorescent switch sensor. The excellent optical stability of OCDs was confirmed by repeating the tests every 5 min (Fig. 3b and Fig. S8, ESI†). The FT-IR spectra (Fig. S9, ESI†) and Raman spectra (Fig. S10, ESI†) of the OCD powder before and after irradiation for 1 h at 254 nm were studied and the results showed that the structure of OCDs was not changed by continuous ultraviolet irradiation. These tests imply its potential in practical applications. Fig. 3c and Fig. S11 (ESI†) exhibit the varied fluorescence intensities of OCDs under different pH conditions, in which the maximal emission intensity at 320 nm was achieved at around pH 8. Fluorescence quenching of OCDs occurs under strong acidic and alkaline conditions, which may be attributed to the fact that the carbon dots are both electron acceptors and electron donors. When the pH is

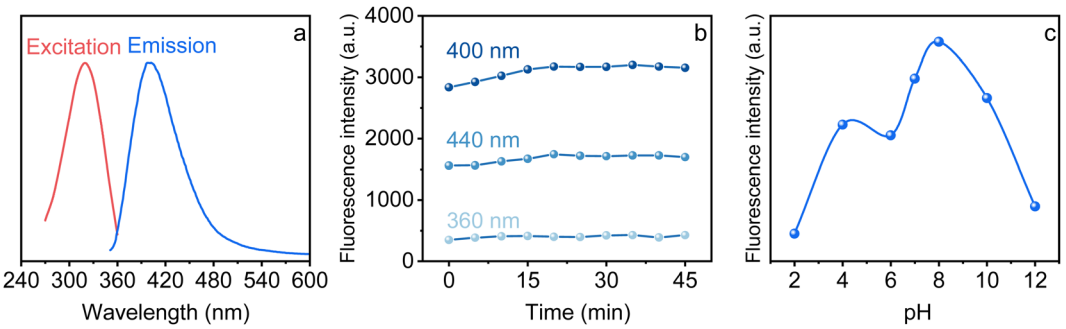

Fig. 3 Fluorescence properties of OCDs. (a) Fluorescence excitation (at 400 nm) and emission (under 320 nm) spectra; (b) fluorescence emission intensities change with time; (c) pH-dependent fluorescence emission intensities.

low or high, the protonation and deprotonation of functional groups on the surface of the carbon dots cause changes in the states of luminescent groups and thus change the fluorescence intensity.[44,45] Regarding the practical conditions, as well as its bright photoluminescence under near-neutral conditions, the follow-up fluorescence measurements were all conducted under neutral conditions (samples were prepared in deionized water).

Specific detection of Fe(III) against Fe(II)

To evaluate the specific recognition ability of OCDs, a ferric ion-containing solution (0.5–75 μM) was added to the OCD dispersion, exhibiting remarkable switch-off fluorescence behavior (Fig. 4a and b). The emission intensity of the solution gradually decreased with the increase in Fe(III) concentration. The maximal quenching efficiency (QE) of 95.9% was achieved with 75 μM of Fe(III). The inset in Fig. 4b demonstrates a good linear relationship between Fe(III) concentration and the QE at 400 nm in the concentration range from 0 to 20 μM. Moreover, the as-prepared OCDs exhibited an ultra-low LOD of 0.440 μM (24.6 ppb) and an outstanding sensitivity of 3.52×10^{-2} μM^{-1}, outperforming many reported fluorescent CDs (Fig. 4c and Table S2, ESI†). Most importantly, this LOD is much lower than the maximum allowable level of 5.4 μM in drinking water according to the U.S. EPA, implying its promising practical drinking water analysis. At the same time, the optical stability of the OCD detection of Fe^{3+} was confirmed by continuous illumination lasting 1 h, and the fluorescence emission spectrum was recorded every 5 min (Fig. S12, ESI†). Additionally, the bonding between OCDs and Fe(III) was revealed using the FT-IR spectra, as shown in Fig. 4d and Fig. S13 (ESI†). In this work, phenolic hydroxyl and carboxyl groups may coordinate with Fe(III) ions, followed by the non-radiative energy transfer between CDs and Fe(III) and resulting in a switch-off fluorescence.[46,47] The coordination behavior was confirmed by the change in the FT-IR spectral features of OCDs after adding Fe(III) ions: the decreasing peaks at 1350 and 765 cm^{-1} can be attributed to the bonding of Fe(III) to –COOH and –OH on OCDs, which is due to the high affinity between Fe(III) and oxygen-containing functional groups. In general, interactions between the surface groups of OCDs and Fe(III) facilitate energy transfer, leading to fluorescence quenching.[48,49] More details are presented in Fig. S13 (ESI†).

Interestingly, when the Fe(III) ion was switched to the Fe(II) ion, the fluorescence quenching effect was turned off, exhibiting I/I_0 of 1.06 at 400 nm even with the Fe(II) concentration as high as 0.1 mM (where I or I_0 represents the fluorescence intensity of OCDs solution with or without Fe(II) ions). Fig. 4e shows the fluorescence spectra of OCDs, which were added to Fe(III) and Fe(II). This suggests that the OCDs can be used for specifically distinguishing Fe(III) from Fe(II). The possible mechanism is that electron configurations of Fe(II) and Fe(III) were significantly different in their energy levels. Typically, based on Hund's rule, the energy level of the half-filled Fe(III) ($3d^5$) is lower than that of Fe(II) ($3d^6$). Meanwhile, the energy level of the excitation state of OCD is located between Fe(III) and Fe(II). Therefore, the energy transfer between the excited OCD and Fe(III) was feasible through non-radiative pathways yet forbidden between the excited OCD and Fe(II). Consequently, effective fluorescence quenching behavior was likely in the presence of Fe(III) but not Fe(II) (Fig. 4f).

More metal ions were adopted to evaluate the specificity of OCDs, including Al(III), Ba(II), Ca(II), Cd(II), Co(II), Fe(II), Hg(II), K(I), Mg(II), Mn(II), Na(I), Ni(II), Pb(II) and Zn(II). As shown in

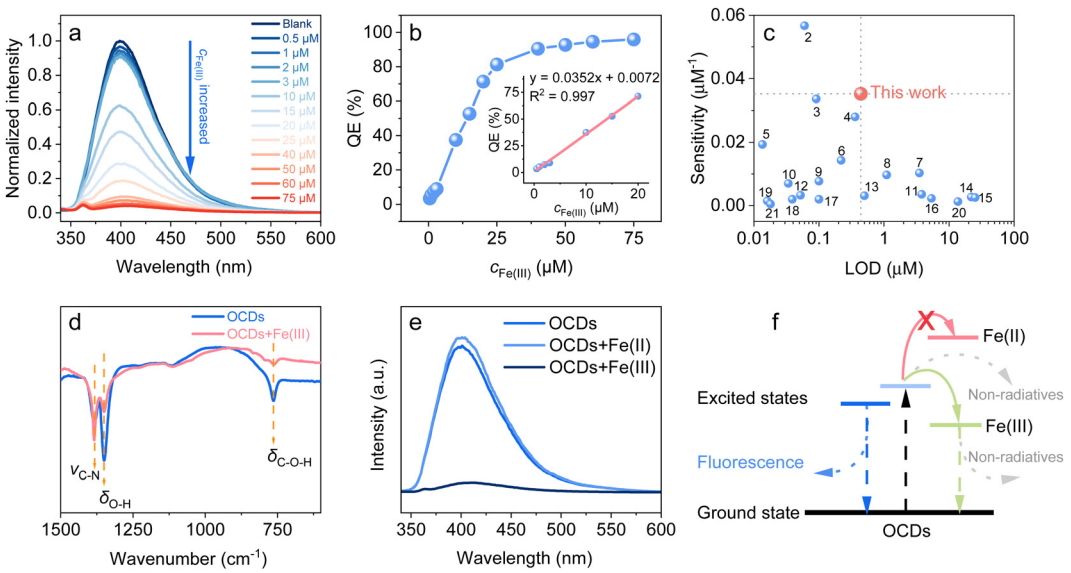

Fig. 4 Fluorescent switching for Fe(III) detection. (a) Fluorescence emission spectra of OCDs with excitation at 320 nm upon the increase in Fe(III) concentration and (b) the corresponding fluorescence quenching efficiencies (inset: the linear relationship between Fe(III) concentration and QE). (c) A comparison of the sensitivity and LOD of OCDs and reported CDs materials based on bottom-up preparation in Fe(III) detection (note: the label of each spot corresponds to the item number in Table S2, ESI†). (d) FT-IR spectra of the OCDs and Fe(III)-OCDs. (e) Comparison of fluorescence emission spectra among OCDs, Fe(III)-OCDs and Fe(II)-OCDs. (f) The proposed mechanism for OCD recognition of Fe(III) in the presence of Fe(II).

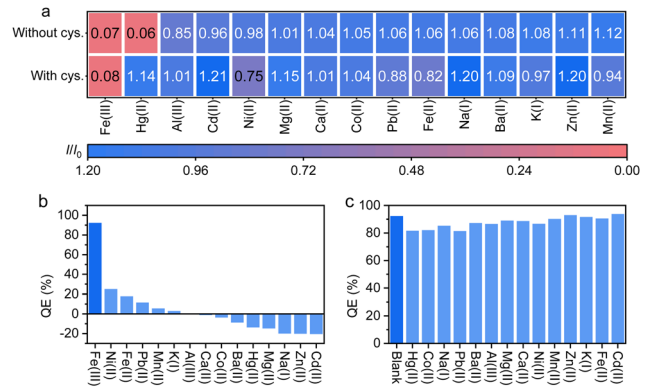

Fig. 5 Specificity and anti-interference performance of the OCDs-based Fe(III) fluorescent switch. (a) A comparison of the fluorescence intensities of OCDs for the detection of various metal ions with and without cysteine. (b) A comparison of fluorescence quenching efficiencies by different metal ions in the presence of cysteine (300 μM); (c) anti-interference tests with the addition of different metal ions to the Fe(III) detection (100 μM) in the presence of cysteine (300 μM).

Fig. 5a and Fig. S14–S28 (ESI†), most of them had negligible effects on the I_0/I ($|I/I_0 - 1| \times 100\% < 15\%$, where I and I_0 represent the intensity with or without metal ions) at 400 nm, except for Hg(II), which implies the excellent anti-interference of OCDs. As for Hg(II), the I_0/I value was merely 0.061 at the concentration of 100 μM (Fig. S28, ESI†), which was similar to Fe(III). Moreover, we found that the specific recognition of Fe(III) as compared to Hg(II) can be realized under the masking effect of cysteine (Fig. S29, ESI†). As shown in Fig. 5a and Fig. S30 (ESI†), the I_0/I values for Fe(III) were 0.077 and 0.065 with and without cysteine, respectively, which indicated that the addition of cysteine hardly affects the detection of Fe(III) (Fig. S29–S43, ESI†). Whereas, the I_0/I values at 400 nm for Hg(II) can be significantly elevated to 1.137 with the addition of cysteine. Besides, the corresponding QE provides evidence of the superior masking effect of cysteine (Fig. 5b). The discussion about the mechanism of the masking effect of cysteine is provided in the ESI.†

To investigate the effects of interferents, various interfering ions (Al(III), Ba(II), Ca(II), Cd(II), Co(II), Fe(II), Hg(II), K(I), Mg(II), Mn(II), Na(I), Ni(II), Pb(II) and Zn(II)) were introduced into the solution of OCDs one by one in the presence of Fe(III) and cysteine (Fig. S44–S58, ESI†). QE was calculated based on the intensity of the corresponding Fe(III)-free sample. As shown in Fig. 5c, the QE of 92.3% can be achieved in the interference-free sample as compared to its Fe(III)-free sample. Expectedly, despite the existing interfering ions, the fluorescence quenching was hardly changed and similar QEs were obtained, which ranged from 81.4% to 93.8%, close to the interference-free result. Notably, the fluorescence intensity with Hg(II) interference can still be quenched by Fe(III), resulting in a QE of 81.6%. These results demonstrated the excellent anti-interference performance of OCDs.

Detection of Fe(III) in real water samples by OCDs as sensors

To evaluate the performance of OCDs for Fe(III) detection in real samples, the performance of the as-prepared OCDs in real

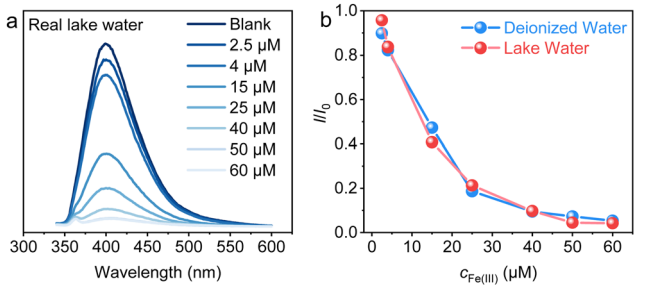

Fig. 6 Fe(III) detection in real lake water. (a) Fluorescence emission spectra of OCDs under excitation at 320 nm for different Fe(III) concentrations in real lake water; (b) plots of fluorescence intensities at different Fe(III) concentrations.

samples was investigated using lake water samples collected from Emerald Lake, Hefei, China. Fig. 6a shows the fluorescence spectra of the OCDs in the lake water with different concentrations of Fe(III) ions. The fluorescence intensity at 400 nm gradually decreased with the increase in the Fe(III) ion concentration, which is similar to that in deionized water (Fig. 6b). The tiny differences between the two conditions are likely caused by the presence of different types of organic and mineral matter in the lake water. The analysis results are shown in Table S3 (ESI†), where it can be seen that the recoveries of Fe^{3+} ions of different concentrations measured by OCDs in real water samples range from 87.5% to 118.1%. A good linear relationship was observed between I/I_0 and $\ln[c_{Fe(III)}]$ in Fig. S59 (ESI†), giving a function of $I_0/I = -0.304 \ln[c_{Fe(III)}] + 1.24$ and a correlation coefficient (R^2) of 0.994. This result reveals the practicability of OCDs in real sample analysis.

Fluorescence quenching mechanism analysis

In general, most fluorescence switching systems can be described quantitatively by the linear Stern–Volmer equation[50] (eqn (4)):

$$\frac{I_0}{I} = 1 + K_{SV}[Q] \quad (4)$$

where I_0 is the fluorescence intensity in the absence of a quencher; I is the intensity when a quencher is present; K_{sv} is the Stern–Vomer quenching constant, also known as the sensitivity of the system, and $[Q]$ is the concentration of the quencher. Nevertheless, this does not seem to match the linear relationship for our Fe(III) fluorescence switching OCDs (Fig. 7a). The possible reason is the formation of a complex between OCDs and Fe(III) ions, assuming the coordination reaction between OCDs and Fe(III) is as follows:

$$* + \text{Fe(III)} \rightleftharpoons *\text{Fe} \quad (5)$$

where * represents the fluorescent binding site (fluorophore) on OCDs; *Fe represents the Fe(III) complex on each fluorescent binding site. The chemical equilibrium constant (K) can be expressed as

$$K = \frac{[*\text{Fe}]_e}{[*]_e \times [\text{Fe(III)}]_e} \quad (6)$$

where $[*\text{Fe}]_e$, $[*]_e$ and $[\text{Fe(III)}]_e$ represent the equilibrium concentration of the complex adduct *Fe, fluorophore * and Fe(III)

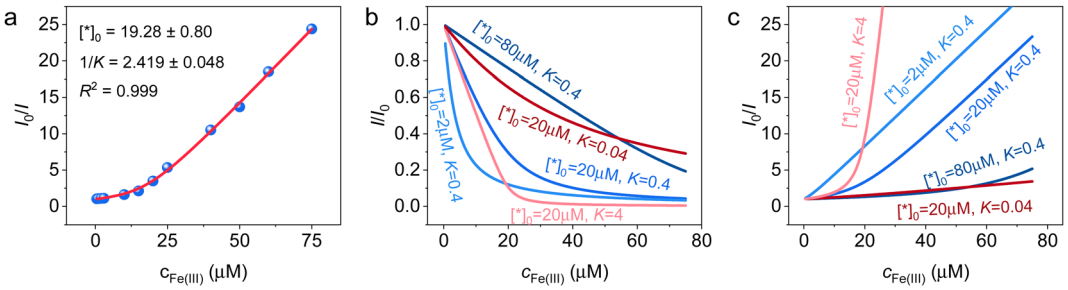

Fig. 7 (a) $I_0/I \sim c_{Fe(III)}$ plot and the corresponding quantitative fitting results according to eqn (8); predicted plots for (b) I/I_0 and (c) I_0/I upon increasing $c_{Fe(III)}$ under different constants.

ions, respectively; $[*]_0$ and $[Fe(III)]_0$ are the initial concentrations of the fluorophore * and Fe(III) ions, respectively. The relative fluorescence intensity (I_0/I) can be given by the relative concentration of fluorophore as follows:

$$\frac{I_0}{I} = \frac{[*]_0}{[*]_e} = \frac{[*]_e + [*Fe]_e}{[*]_e} = 1 + \frac{[*Fe]_e}{[*]_e \times [Fe(III)]_e} \times [Fe(III)]_e = 1 + K \times [Fe(III)]_e \quad (7)$$

Therefore, only when $[Fe(III)]_e \approx [Fe(III)]_0$ can I_0/I be approximately described by the Stern–Volmer equation. Eqn (6) can be further derived as follows:

$$K = \frac{[*Fe]_e}{([*]_0 - [*Fe]_e \times ([Fe(III)]_0 - [*Fe]_e))} \quad (8)$$

$$[*Fe]_e^2 - \left([*]_0 + [Fe(III)]_0 + \frac{1}{K}\right) \times [*Fe]_e + [*]_0 \times [Fe(III)]_0 = 0 \quad (9)$$

$[*Fe]_e$ can be calculated using the following expression:

$$[*Fe]_e = \frac{[*]_0 + [Fe(III)]_0 + \frac{1}{K} \sqrt{\left([*]_0 + [Fe(III)]_0 + \frac{1}{K}\right)^2 - 4 \times [*]_0 \times [Fe(III)]_0}}{2} \quad (10)$$

Therefore, I_0/I can be expressed as follows:

$$\frac{I_0}{I} = \frac{[*]_0}{[*]_e} = \frac{[*]_0}{[*]_0 - [*Fe]_e} = \frac{2 \times [*]_0}{[*]_0 - [Fe(III)]_0 - \frac{1}{K} + \sqrt{\left([*]_0 + [Fe(III)]_0 + \frac{1}{K}\right)^2 - 4 \times [*]_0 \times [Fe(III)]_0}} \quad (11)$$

The corresponding fitting result has been demonstrated in Fig. 7a, giving $[*]_0$ = 19.3 μmol L^{-1} and K = 0.413, which agree well with the experimental data.

We also drew the $I_0/I \sim c_{Fe(III)}$ and $I/I_0 \sim c_{Fe(III)}$ curves according to eqn (11), and predicted the trend of the corresponding curves under different fluorophore concentrations $[*]_0$ and reaction equilibrium constant K values, as shown in Fig. 7b and c. It was observed that reducing $[*]_0$ or increasing K (that is, essentially the affinity between the fluorophore and Fe(III) ions) can effectively improve the sensitivity of Fe ion fluorescence detection, obtaining a steeper curve slope. Alternatively, increasing $[*]_0$ or decreasing K can expand the quasi-linear range and afford a wider working range. This provides us with a design roadmap for the metal ion fluorescence switch materials based on a complex formation quenching mechanism.

Fluorescence cell imaging in plant cells

To examine the feasibility of the fluorescent OCDs on cell imaging, potatoes (Fig. 8a), bean sprouts (Fig. 8b) and winter squash (Fig. 8c) were selected as cell models. To avoid fluorescence interference, cell imaging tests were performed on chlorophyll-free cells. Compared to pristine plant cells (Fig. 8d–f), bright blue fluorescence was observed for the three kinds of plant samples after treatment with the OCD solution (Fig. 8g–i), which suggests that the OCDs can smoothly enter plant cells, and proves the great biocompatibility of OCDs. Moreover, after absorbing Fe(III) ions, dramatic fluorescence quenching was observed for all three samples(Fig. 8j–l). This not only further verifies the outstanding Fe(III) fluorescence switching performance of OCDs, but also reveals the great potential of OCDs as probes for cellular fluorescence imaging.

Conclusions

The following conclusions were drawn:

(1) OCDs derived from oxytetracycline, with a uniform size (*ca.* 2.04 nm), nitrogen-dopant and rich hydroxyl-/carboxyl- groups, were successfully fabricated *via* a bottom-up HTC approach.

(2) OCDs can be used to specifically distinguish Fe(III) from Fe(II), achieving an acceptable limit of detection as low as 0.440 μM (24.6 ppb) and the second highest sensitivity of 3.52 × 10^{-2} μM^{-1} among reported CD materials.

(3) The complexing mechanism has been proved by the proposed numerical model, providing a design roadmap for

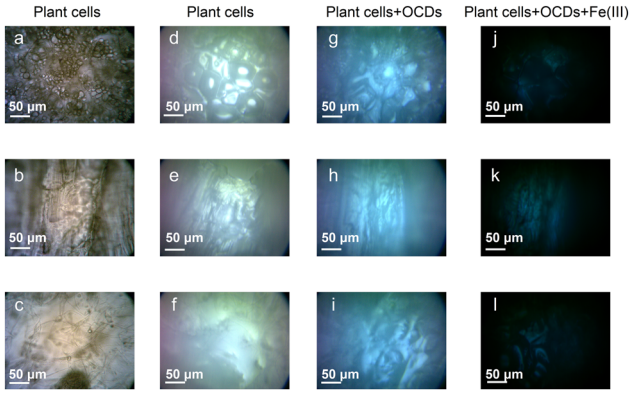

Fig. 8 Plant cell images in bright field: (a) potatoes, (b) bean sprouts and (c) winter squash. The corresponding cell images under a fluorescence microscope: (d) potatoes, (e) bean sprouts, (f) winter squash, (g) potatoes with OCDs, (h) bean sprouts with OCDs, (i) winter squash with OCDs, (j) potatoes with OCDs and Fe(III), (k) bean sprouts with OCDs and Fe(III) and (l) winter squash with OCDs and Fe(III). Magnification: 3200 times.

the metal ion fluorescence switch materials based on a complex formation quenching mechanism.

(4) OCDs can further expand their usefulness and feasibility in the specific detection of Fe(III) in real water environments, as well as living plant cells.

(5) This is a feasible strategy for recycling environmentally-risky waste antibiotics, such as oxytetracycline.

Conflicts of interest

The authors declare that they have no known competing financial interests or personal relationships that could have appeared to influence the work reported in this paper.

Acknowledgements

The authors gratefully acknowledge the financial support of the NSFC (22178339), and also the Hundred Talents Program (A) of Chinese Academy of Sciences (2019), the Guangdong Basic and Applied Basic Research Foundation (2021A1515110069), the fellowship of China Postdoctoral Science Foundation (2021M690151), the Guangdong Provincial Key Laboratory of New and Renewable Energy Research and Development (2021000037) and the Basic Research Program of Guangzhou City (202102020866).

Notes and references

1 J. Zhu, H. Chu, T. Wang, C. Wang and Y. Wei, *Microchem. J.*, 2020, **158**, 105142.
2 R. Atchudan, T. N. J. I. Edison, K. R. Aseer, S. Perumal, N. Karthik and Y. R. Lee, *Biosens. Bioelectron.*, 2018, **99**, 303–311.
3 R. Atchudan, T. N. J. I. Edison, K. R. Aseer, S. Perumal and Y. R. Lee, *Colloids Surf., B*, 2018, **169**, 321–328.
4 Z. Xie, J. Sun, Z. Zhou and S. Xia, *Mater. Technol.*, 2021, **55**, 141–147.
5 R. Bandi, R. Dadigala, B. R. Gangapuram, F. K. Sabir, M. Alle, S. H. Lee and V. Guttena, *Mikrochim. Acta*, 2020, **187**, 30.
6 O. A. Aladesuyi and O. S. Oluwafemi, *Heliyon*, 2023, **9**, e15904.
7 W. Ji, Z. Zhu, S. Dong, J. Nie and B. Du, *Sensors*, 2019, **19**, 4223.
8 X. Zhang, C. Li, S. Zhao, H. Pang, Y. Han, X. Luo, W. Tang and Z. Li, *Opt. Mater.*, 2020, **110**, 110461.
9 A. M. Khan, S. Khizar, S. A. Khan, S. Ali, A. Shah, M. F. Nazar, F. J. Iftikhar, F. Shah, R. A. Khan and A. R. Khan, *J. Mol. Liq.*, 2020, **313**, 113599.
10 S. Yin and Z. Ma, *Sens. Actuators, B*, 2019, **281**, 857–863.
11 M. Asmari, A. M. Abdel-Megied, L. Michalcová, Z. Glatz and S. El Deeb, *Microchem. J.*, 2020, **154**, 104556.
12 F. Wu, M. Yang, H. Zhang, S. Zhu, X. Zhu and K. Wang, *Opt. Mater.*, 2018, **77**, 258–263.
13 J. Liu, D. Li, K. Zhang, M. Yang, H. Sun and B. Yang, *Small*, 2018, **14**, 1703919.
14 J. Yang, W. Chen, X. Liu, Y. Zhang and Y. Bai, *Mater. Res. Bull.*, 2017, **89**, 26–32.
15 H. Wu, J. Jiang, X. Gu and C. Tong, *Microchim. Acta*, 2017, **184**, 2291–2298.
16 J. Athinarayanan, A. A. Alshatwi and V. Subbarayan Periasamy, *Carbohydr. Polym.*, 2020, **235**, 115961.
17 Y. Wang, Y. Man, S. Li, S. Wu, X. Zhao, F. Xie, Q. Qu and W. S. Zou, *Spectrochim. Acta, Part A*, 2020, **226**, 117594.
18 J. Athinarayanan, S. A. Almaiman, L. N. Al-Harbi, V. S. Periasamy and A. A. Alshatwi, *J. King Saud Univ., Sci.*, 2021, **33**, 101584.
19 Y. Man, Z. Li, W.-L. Kong, W. Li, W. Dong, Y. Wang, F. Xie, D. Zhao, Q. Qu and W.-S. Zou, *Microchem. J.*, 2020, **159**, 105338.
20 Z. Fu, M. Yao, X. Niu and F. Cui, *Sens. Actuators, B*, 2016, **226**, 486–494.
21 J. Zhou, Y. Yang and C.-Y. Zhang, *Chem. Rev.*, 2015, **115**, 11669–11717.
22 J. Shen, S. Shang, X. Chen, D. Wang and Y. Cai, *Mater. Sci. Eng., C*, 2017, **76**, 856–864.
23 R. Atchudan, T. N. J. I. Edison, S. Perumal, R. Vinodh and Y. R. Lee, *J. Mol. Liq.*, 2019, **296**, 111817.
24 Y. Zhou, Y. Liu, Y. Li, Z. He, Q. Xu, Y. Chen, J. Street, H. Guo and M. Nelles, *RSC Adv.*, 2018, **8**, 23657–23662.
25 Y. Zhang, X. Yang, Y. Pu, W. Cheng, S. Lin, Z. Shao and X. Liao, *J. Fluoresc.*, 2019, **29**, 541–548.
26 R. Wang, L. Jiao, X. Zhou, Z. Guo, H. Bian and H. Dai, *J. Hazard. Mater.*, 2021, **412**, 125096.
27 M. Zulfajri, G. Gedda, C.-J. Chang, Y.-P. Chang and G. G. Huang, *ACS Omega*, 2019, **4**, 15382–15392.
28 Z. Xie, X. Sun, J. Jiao and X. Xin, *Colloids Surf., A*, 2017, **529**, 38–44.
29 W. Wang, J. Peng, F. Li, B. Su, X. Chen and X. Chen, *Microchim. Acta*, 2018, **186**, 32.
30 D. Liu, M. Li, X. Li, F. Ren, P. Sun and L. Zhou, *Chem. Eng. J.*, 2020, **387**, 124008.
31 R. Atchudan, S. Chandra Kishore, P. Gangadaran, T. N. Jebakumar Immanuel Edison, S. Perumal, R. L. Rajendran, M. Alagan, S. Al-Rashed, B. C. Ahn and Y. R. Lee, *Environ. Res.*, 2022, **204**, 112365.

32 S. Wang, S. Liu, J. Zhang and Y. Cao, *Talanta*, 2019, **198**, 501–509.
33 Z. Chen, X. Xu, D. Meng, H. Jiang, Y. Zhou, S. Feng, Z. Mu and Y. Yang, *J. Fluoresc.*, 2020, **30**, 1007–1013.
34 M. Lu, Y. Duan, Y. Song, J. Tan and L. Zhou, *J. Mol. Liq.*, 2018, **269**, 766–774.
35 P. Krishnaiah, R. Atchudan, S. Perumal, E.-S. Salama, Y. R. Lee and B.-H. Jeon, *Chemosphere*, 2022, **286**, 131764.
36 J. Zheng, Y. Xie, Y. Wei, Y. Yang, X. Liu, Y. Chen and B. Xu, *Nanomaterials*, 2020, **10**, 82.
37 S. Chandra, A. R. Chowdhuri, D. Laha and S. K. Sahu, *Luminescence*, 2018, **33**, 336–344.
38 R. Atchudan, P. Gangadaran, S. Perumal, T. N. J. I. Edison, A. K. Sundramoorthy, R. L. Rajendran, B.-C. Ahn and Y. R. Lee, *J. Clust. Sci.*, 2023, **34**, 1583–1594.
39 H. Qi, M. Teng, M. Liu, S. Liu, J. Li, H. Yu, C. Teng, Z. Huang, H. Liu, Q. Shao, A. Umar, T. Ding, Q. Gao and Z. Guo, *J. Colloid Interface Sci.*, 2019, **539**, 332–341.
40 T. V. Huynh, N. T. N. Anh, W. Darmanto and R.-A. Doong, *Sens. Actuators, B*, 2021, **328**, 129056.
41 L. J. Mohammed and K. M. Omer, *Sci. Rep.*, 2020, **10**, 3028.
42 X. Chu, T. Chen and Y. Cao, *Microchem. J.*, 2022, **177**, 107255.
43 S. Zhu, Q. Meng, L. Wang, J. Zhang, Y. Song, H. Jin, K. Zhang, H. Sun, H. Wang and B. Yang, *Angew. Chem., Int. Ed.*, 2013, **52**, 3953–3957.
44 B. Shi, L. Zhang, C. Lan, J. Zhao, Y. Su and S. Zhao, *Talanta*, 2015, **142**, 131–139.
45 X. Chu and Y. Cao, *New J. Chem.*, 2021, **45**, 20575–20585.
46 M. Picard, S. Thakur, M. Misra and A. K. Mohanty, *RSC Adv.*, 2019, **9**, 8628–8637.
47 Q. Ye, F. Yan, Y. Luo, Y. Wang, X. Zhou and L. Chen, *Spectrochim. Acta, Part A*, 2017, **173**, 854–862.
48 R. Atchudan, T. N. J. I. Edison, D. Chakradhar, S. Perumal, J.-J. Shim and Y. R. Lee, *Sens. Actuators, B*, 2017, **246**, 497–509.
49 Y. Zhou, G. Chen, C. Ma, J. Gu, T. Yang, L. Li, H. Gao, Y. Xiong, Y. Wu, C. Zhu, H. Wu, W. Yin, A. Hu, X. Qiu, W. Guan and W. Zhang, *Spectrochim. Acta, Part A*, 2023, **293**, 122414.
50 N. Li, Q. Xu, X. Xia, L. Wang, J. Lu and X. Wen, *Mater. Chem. Phys.*, 2009, **114**, 339–343.